IEEE Photonics Journal
An IEEE Photonics Society Publication

Open Access

High-Performance Electro-Optic Manipulation by Plasmonic Light Absorber With Nano-Cavity Field Confinement

Volume 13, Number 3, June 2021

Guiqiang Liu
Qizhao Wu
Xiaoshan Liu
Xuefeng Zhan
Guolan Fu
Chaojun Tang
Zhengqi Liu

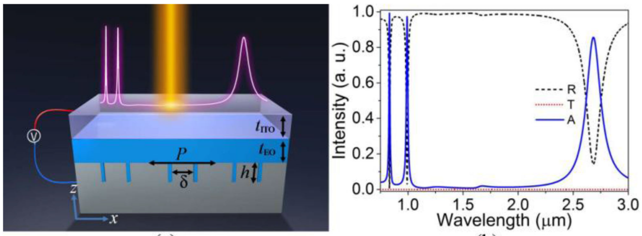

(a) (b)

DOI: 10.1109/JPHOT.2021.3073686

High-Performance Electro-Optic Manipulation by Plasmonic Light Absorber With Nano-Cavity Field Confinement

Guiqiang Liu,[1] Qizhao Wu,[1] Xiaoshan Liu,[1] Xuefeng Zhan,[1] Guolan Fu,[1] Chaojun Tang,[2] and Zhengqi Liu[1]

[1]College of Physics and Communication Electronics, Jiangxi Normal University, Nanchang 330022, Jiangxi, China
[2]College of Science, Zhejiang University of Technology, Hangzhou 310023, China

DOI:10.1109/JPHOT.2021.3073686

Manuscript received March 15, 2021; revised April 8, 2021; accepted April 13, 2021. Date of publication April 16, 2021; date of current version April 29, 2021. This work was supported in part by the National Natural Science Foundation of China under Grants 51761015, 62065007, 11804134, 11104136, in part by the Natural Science Foundation of Jiangxi Province under Grants 20202BBEL53036 and 20202BAB201009, and in part by the Natural Science Foundation of Zhejiang Province under Grant LY14A040004. Corresponding authors: Guolan Fu, Chaojun Tang, Zhengqi Liu (e-mail: glfu@jxnu.edu.cn; chaojuntang@zjut.edu.cn; zliu@jxnu.edu.cn).

Abstract: Narrowband light absorber with multi-band plasmonic resonances is numerically investigated for high-performance electrical manipulation via introducing the electro-optic (EO) medium in the slit array based grating structure. A maximal absorption efficiency of 99.5% is achieved. The spectral shift sensitivity reaches 0.99 nm/V. Besides, the large spectral intensity change is also obtained due to the use of sharp resonances, which therefore ensures the high signal-to-noise ratio for the manipulation process. It is observed that the strong surface plasmon resonance and the localized optical cavity modes can introduce the differential responses for the multiple modes under the optical adjusting process and also for the EO manipulation process. These features not only contribute to produce the new EO modulator platforms based on the light absorbers but also pave new ways for the cavity-enhanced high-performance EO operation. Moreover, the absorption properties can be well maintained in a wide range of the structural parameters, indicating the high tolerance of the fabrication process. The findings can pave new insights into the high-performance manipulations via the narrowband absorbers with strong electromagnetic field enhancement and hold wide applications in dynamic switching, filtering, displaying, etc.

Index Terms: Plasmonics, light absorber, electro-optic, localized optical cavity.

1. Introduction

Plasmonic resonances have been widely developed for numerous applications including solar light harvesting and energy conversion [1]–[3], high-performance sensing and detection [4]–[7], deep-subwavelength nano-optics [8]–[10], and nonlinear optics [11]–[13] due to the intrinsic strong electromagnetic field enhancement via the localized electrons oscillations in the nano-structured resonators. The light flow trapped in the resonators, usually by the metallic nano-structures, could be transformed to the evanescent wave in the limited spatial area close to the metal surface, which holds the great contributions for efficient light-matter interactions.

On the other hand, plasmonic resonances and strong electromagnetic wave coupling effects have been employed for light absorption. In 2008, perfect microwave absorption has been realized via the design of metal-insulator-metal triple-layer meta-material [14], which was observed to support both the electric and magnetic resonances by the split metal ring resonator and the top and bottom metal parts separated by the middle dielectric buffer layer. Since then, perfect absorbers have been exploited with powerful ways to enhance the electromagnetic wave trapping and the solar energy related techniques [15]–[17], subtractive filtering [18], high signal-to-noise ratio sensing and detection [19]–[22], and new emerged optoelectronic devices [23]–[25]. Absorbers with broadband and narrowband are both desirable for applications. For instance, broadband absorption, even the absorption wavelength range covering the full-spectrum of the solar energy, is the key point for the applications in the solar energy techniques including the desalination [26] and photo-thermal steam generation [27]–[29]. A typical way to achieve the broadband absorption is to utilize multiple resonators combined in the unit cell to produce a series of resonances in the wide wavelength range [25],[30]–[33], which therefore leads to the formation of an expanded spectral absorption band. As for the narrowband absorption, several ways have been utilized to improve the spectral quality factor. Hybridized coupling between the different resonances in the composite structures is a common method to achieve sharp resonant absorption [34],[35]. Optical cavity assisted metal films [36] and oblique excitation in the corrugated metal film structures [37] have also been used for narrowband resonances. Asymmetric metallic nano-structures also produced the sharp resonances [38], [39] due to the coupling between the resonances supported by the adjacent resonators.

Via tuning the structural features, it is well-known that the plasmonic resonances can be artificially manipulated. Nevertheless, in contrast to the need of changing the structure parameters, the external manipulation for the absorption properties via the optical operations could be a better choice since it is more feasible to achieve the time-saving manipulation. For instance, due to the polarization-dependent absorption behaviors, it is easy to artificially tune the absorption efficiency for the absorber via changing the polarization state of the illumination source [40],[41]. Otherwise, via using the phase change materials, resonant absorption intensity can be strongly manipulated, showing the switching operations for functional modulators [42],[43]. Nevertheless, in these operation processes, it is not easy or unable to tune the resonant wavelengths. That is, it is still with the need to carry out the different design and fabrication processes for the systems worked at the different wavelength ranges.

In this work, we propose and numerically demonstrate a facile strategy for the multi-band high-performance electric-adjusting platform via using a narrowband light absorber, which ensures the high absorption and the strong local field enhancement by the plasmonic cavity resonances. In contrast to the complex structural features formed by the multiple metallic layers or resonators in the previous reports [25],[38],[44], only a slit cavity assisted metal grating is used to produce the plasmonic resonances and realize the light flow confinement. Otherwise, the absorber is an open system due to the transparent dielectric medium used as the cover film, which therefore enables the highly spectral ratio for the absorption and reflective states at the operation or the standby states. These findings are impressive for applications in active optoelectronic devices.

2. Geometric Parameters and Simulation Methods

Herein, we use a metal-dielectric composite structure to act as the narrowband absorber. As shown in Fig. 1(a), the absorber only consists of triple layers, the bottom substrate of metal film grating with nano-slits array, the middle packing layer of the EO medium, the top transparent conducting layer of the indium tin oxides (ITO) film. Via tuning the applied voltage, the EO medium can be changed to then introduce the related spectral response. Silver with a relative low absorption loss is chosen as the metal substrate and the plasmonic material. Lithium tantalite ($LiTaO_3$) is used as the functional layer since its refractive index n can be artificially changed following the relationship $n = n_0 + 0.5{n_0}^3 E\eta$ due to the Pockels effect [45],[46]. The ordinary index of $LiTaO_3$ is $n_0 = 2.175$ under the x-polarized (TM polarization) illumination. The electric field E is related to the applied voltage V_a

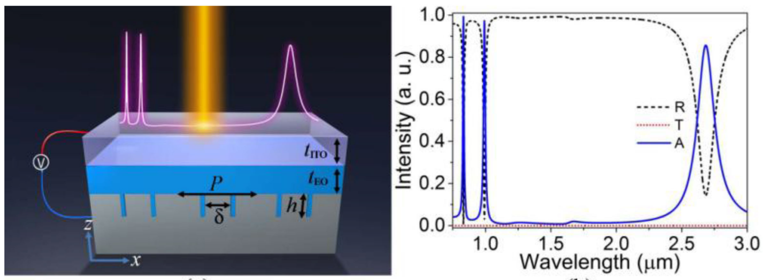

(a) (b)

Fig. 1. (a) Schematic diagram of the narrowband plasmonic absorber and the electro-optic manipulation. (b) Spectral reflection, transmission, absorption of the absorber.

and the film thickness of the EO is defined as t_{EO}. η is the EO efficiency. All the computations are carried out via using the finite-difference time-domain method. The dielectric permittivity of the silver is obtained from the experimental data [47]. In the simulation, the spectral reflection *R*(λ) and transmission *T*(λ) are obtained directly via the monitors. The spectral absorption *A*(λ) is calculated via the definition of *A*(λ) $=$ 1 - *R*(λ) - *T*(λ). In order to wholly cancel the transmission, the film thickness of the silver is set to be 300 nm. Paired nano-slits with the height *h* and the displacement distance δ are introduced to locate in the surface of the silver to form the plasmonic cavity structure. The period *P* of the array is set to be 600 nm. The *h* and δ are both equal to 100 nm. The width of the nano-slit is set to be 10 nm. The thicknesses of the EO film and the ITO layer are 50 nm. It should be noted that the nano-slits can be realized via the standard atomic layer lithography technique [48], super-resolution laser lithography [49], and the cascade domino lithography [50], which have been developed in these years and demonstrated for sub-5 nm nano-gap and slit fabrication. For instance, split-wedge antennas with sub-5 nm nano-gaps were realized based on these techniques [48], [51].

Fig. 1(b) shows the spectral *R*, *T*, *A* of the absorber under normal incidence. It is observed that the light transmission is close to 0, indicating the extremely transmission inhibition. Two sharp reflection dips are observed at the shorter wavelength range. One anti-reflection band occurs at the longer wavelength range. In the other spectral range, the reflection is close to 1. Moreover, the spectral curve is flat, indicating a large spectral ratio for the anti-reflection and high reflection ranges. As a result, a tri-band absorption phenomenon is achieved in a near-zero absorption spectral range. At $\lambda_1 =$ 0.831 μm, the *A* reaches 99.5%. The spectral *Q* factor is up to 88.4. At $\lambda_2 =$ 0.992 μm, the *A* reaches 97.5%. The spectral *Q* factor is still up to 66.1. At $\lambda_3 =$ 2.682 μm, the *A* reaches 85.6%. The spectral *Q* factor is 16.9. These features indicate the achievement of the three-band resonant absorption.

3. Results, Analysis and Discussion

For the resonant absorption peaks (λ_1-λ_3), the normalized electric and magnetic field intensity distributions are shown in Fig. 2. For the absorption peak at λ_1, the electric field is strongly located in the slit areas and the magnetic field is located on the surface areas (Fig. 2(a)), which indicate the excitation of the propagating surface plasmon resonance by the metal grating. At λ_2 and λ_3, the electric and magnetic fields are both confined in the slit areas. For the former one, the field patterns are clearly observed with two parts as shown in Fig. 2(b). The field patterns seem to be only one part for the latter one. These characteristics confirm the excitation of the 2$^{\mathrm{th}}$ and 1$^{\mathrm{th}}$ cavity modes [52]–[56] via the nano-slit assisted metal grating structure for the resonant absorption at λ_2 and λ_3, respectively.

Based on this plasmonic cavity resonances assisted light absorber, we further investigate the artificially tunable features via using the applied voltage V_{a}, which could lead to the influence on the EO film. As the applied voltage varies, the index of the surrounding medium alters. As a result,

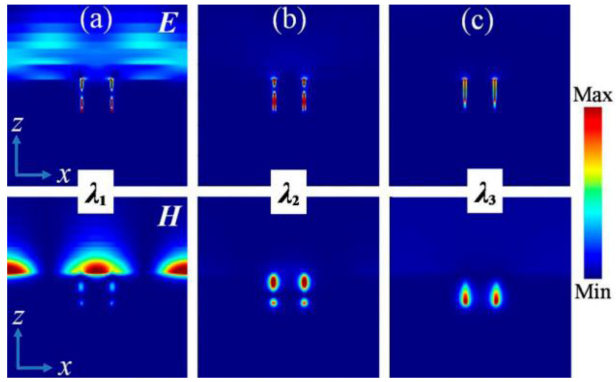

Fig. 2. (a)-(c) Normalized electric (top) and magnetic (bottom) field intensity distributions for the resonant absorption peaks at λ_1-λ_3, respectively.

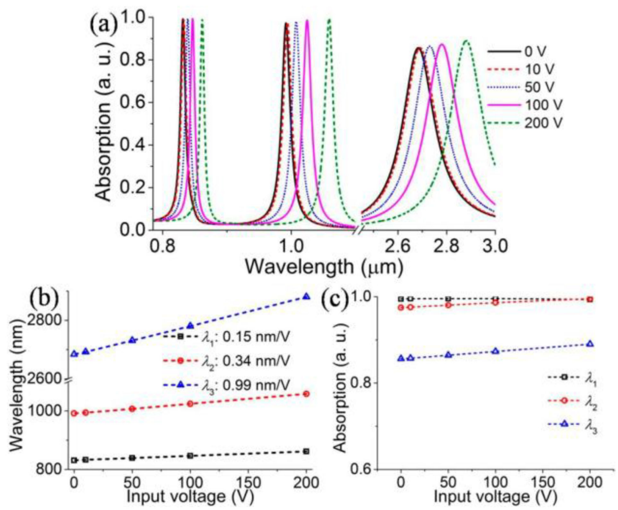

Fig. 3. (a) Spectral evolution for the absorption under a tuning of the voltage. (b) Plotted wavelength positions for the peaks at λ_1-λ_3 as a function of the input voltage. (c) Absorption efficiency for the peaks during the manipulation process.

the resonant wavelengths can show high sensitivity to the change by the strong localized field enhancement. As shown in Fig. 3(a), the resonant absorption peaks show continuous red-shifts when the applied voltage V_a is increased from 0 to 200 V. Fig. 3(b) shows the plotted wavelength positions of the tri-band absorption peaks as a function of the input voltage. In the tuning range, the positions for these peaks can be linearly fitted. As a result, the spectral tunable sensitivity *S* can be defined as $\delta\lambda/\delta V_a$. The spectral wavelength shift *S* for these peaks reach 0.15 nm/V, 0.34 nm/V and 0.99 nm/V. It is observed that the sensitivity for the resonant peaks (λ_2, λ_3) enabled by the plasmonic cavity modes are much higher than the propagating surface plasmon based resonant band (λ_1).

In order to achieve a better description for this spectral shift related EO modulation performance, we then use a wavelength-free sensitivity S_λ, which is defined as $S_\lambda = \delta\lambda/\lambda/\delta V_a$. The modulation sensitivity is $S_{\lambda 1} = 1.8\times10^{-4}$, $S_{\lambda 2} = 3.4\times10^{-4}$, and $S_{\lambda 3} = 3.7\times10^{-4}$ for the tri-band peaks at λ_1-λ_3, respectively. The results also confirm the strongly improved modulation sensitivity for the cavity resonances based absorption peaks. During the modulation of the operation positions, the spectral absorption efficiency for the peaks is also considered. As shown in Fig. 3(c), the absorption values seem to be insensitive to the voltage. Only a slight intensity fluctuation occurs. It confirms the high stability of the high absorption during the manipulation operation for this absorber platform.

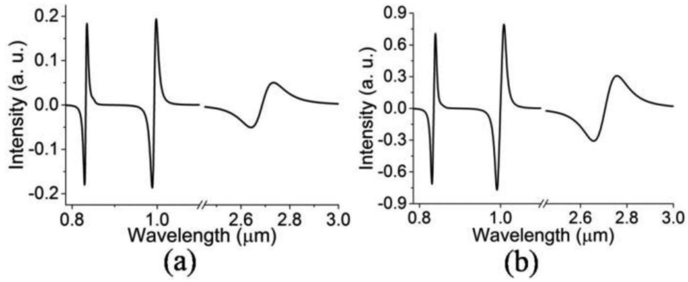

Fig. 4. (a), (b) Plotted spectral intensity changes as a function of the wavelengths after the voltage increased to 10 V and 50 V in comparison with that of the origin curve without the voltage operation, respectively.

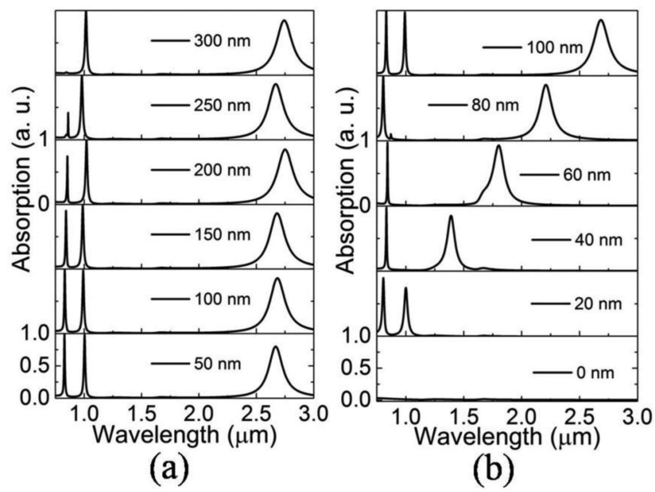

Fig. 5. Absorption curves for the absorber formed under different values of the δ (a) and slit height (b).

During the EO manipulation process, another factor for the performance could be considered besides the spectral shift sensitivity. The related intensity changes or differences are very significant during the tuning operation at the resonant wavelengths, which can hold the high signal-to-noise ratio for the operations. Herein, we take the spectral intensity difference by the definition of $\delta A = A_{Va}$ - A_0. The high δA can ensure the large signal-to-noise ratio for the manipulation. Fig. 4(a) shows the absorption difference intensity for the system after adding a voltage of 10 V. The curve clearly presents the high intensity changes for the tri-band absorption. In particular, the intensity change is close to 20% for the absorption peaks at λ_1 and λ_2 due to the sharp resonant modes. For the case by using an applied voltage of 50 V, the spectral intensity curve shows a much higher difference in comparison with the system before the EO manipulation. For instance, at λ_2, the intensity change reaches 79% (Fig. 4(b)). These features indicate the highly spectral intensity changes can be achieved simultaneously with the spectral shift by the EO manipulation.

Following, the absorption properties under the different structural parameters and the electromagnetic excitations are investigated. Fig. 5(a) shows the absorption curves under different values of the displacement δ for the two slits. It is observed that the sharp resonant absorption bands can be well maintained in a wide range of the δ. Nevertheless, the absorption peak at the shorter wavelength range becomes weak and even be disappeared when the δ is up to 300 nm. With increase the height of the nano-slits from 0 nm to 100 nm (Fig. 5(b)), the absorption curves are observed to be changed noticeably. No absorption peak is observed when there is no slit in the structure. The absorption peak at the longer wavelength range shows a continuous red shift with the increase of the height. This mainly results from the cavity mode occurred at the wavelengths

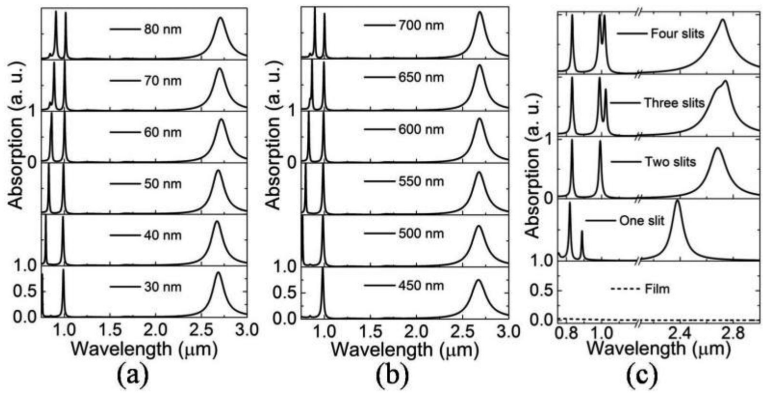

Fig. 6. Absorption evolution under a tuning of the thickness of the EO film (a), the lattice period of the grating (b), and the number of the slits (c).

related to the slit's height. The sharp absorption peaks seem to be very sensitive to the height due to the higher order cavity mode with the need of the suitable height for the resonance [53],[55],[56]. For instance, the 2^{th} mode can be efficiently excited when the height is close to 50 nm or 100 nm. These findings suggest the high stability and high tunability for the absorption behaviors via the different parameters.

Fig. 6(a) shows the absorption evolution for the system by tuning the thickness of the EO film from 30 nm to 80 nm. It is observed that the main features including the high absorption efficiency and the narrowband modes are maintained very well in a wide range of the film thickness. That is, the resonant absorption behaviors mainly result from the plasmonic resonances by the metal slit cavities, suggesting the relatively weak relevant to the EO film. As shown in Fig. 6(b), the resonant absorption can also be well retained when the lattice period is increased from 450 nm to 700 nm. That is, the absorption spectrum can be achieved in a wide range of the lattice size. The absorption curves of the flat metal-dielectric structure, without the slits, and the structure with only one slit in the unit cell are shown in Fig. 6(c). It is observed that rather weak absorption for the flat film structure due to the high reflection by the metal film substrate. For the system formed by one slit in the unit cell, tri-band absorption is also observed. Nevertheless, the absorption at the shorter wavelength range is both less than 80% despite it is very larger for the peak at the longer wavelength range. The results also confirm that the introduced nano-slits in the metal film are with strong contribution to the high absorption for the multi-band absorber. With increasing the number of the slits from one to four, two main features can be observed. The second absorption band becomes stronger and stronger. Moreover, it is splited into two sub-peaks. Otherwise, the spectral red-shift is obtained. These mainly result from the formation of the de-generation of resonant modes by the coupled cavities. Therefore, the number of the slits can also introduce new approaches for the manipulation for the absorption behaviors.

Fig. 7(a) shows the absorption evolution as a function of the incident angle under the TM polarization (electric field along *x*-direction). Via tuning the angle from 0^o to 60^o, the mapping picture shows three main features. One is the highly stability of the positions for the absorption bands at λ_2 and λ_3. The other is the strong dispersion of the absorption at λ_1, which is changed to be two bands under the oblique excitation. This behavior mainly results from the dispersion of the surface plasmon polaritons by the metal film under the grating coupling condition. Moreover, it also interacts with the 2^{th} cavity mode under the large angle close to 30^o. The third one is the slightly weakened absorption efficiency for the peaks under a large angle above 50^o. These features confirm the differential responses for the modes. For instance, it is angle insensitive for the cavity modes based absorption peaks. Nevertheless, it is angle sensitive for the propagating surface plasmon resonance based absorption band. The differential phenomenon can pave a way to tune the resonant absorption peaks separately. The polarization-dependant absorption is observed for

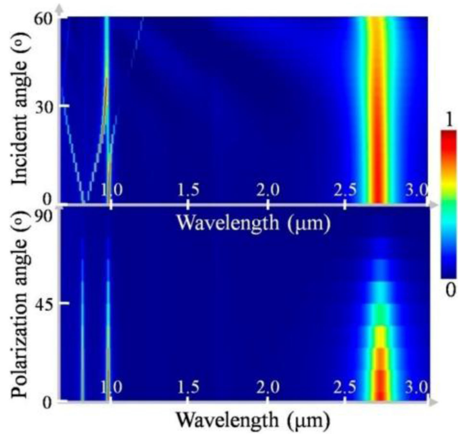

Fig. 7. Absorption mapping for the absorber via tuning the incident angle and the polarization angle.

the grating based absorber via tuning the polarization angle as shown in Fig. 7(b). The absorption efficiency for the tri-band continuously becomes weak when the polarization angle is increased from 0° (TM) to 90° (TE). This mainly results from the low-symmetry of the grating structure. The absorption efficiency can be theoretically modeled by the classical Malus law as a function of the polarization state.

4. Conclusion

In summary, we have proposed and numerically demonstrated a facile strategy for achieving light absorber based EO modulator. Thanks to the strongly localized electromagnetic field effects by the plasmonic cavities in the metal film, a tri-band near-infrared absorber with a maximal absorption efficiency of 99.5% is achieved. Meanwhile, due to the introduction of the EO medium in the resonant structure, high-performance EO modulation is realized. The spectral shift sensitivity reaches 0.99 nm/V during the electrical adjusting operation. Simultaneously, the absorption can be kept in a high level. Besides the high spectral shift sensitivity, the large spectral intensity change is also obtained due to the sharp resonances, which therefore ensures the high signal-to-noise ratio for the manipulation process. These features not only introduce the new EO modulator platform but also pave new ways for the cavity-enhanced high-performance EO operation. Moreover, the absorption properties can be well maintained in a wide range for the structural parameters, indicating the high tolerance of the fabrication process. These impressive results can hold wide applications for the anti-reflective and high absorption EO adjusting components, the artificial light flow filtering and switching operations, etc.

Conflicts of interest

The authors declare no competing financial interest.

References

[1] K. R. Catchpole, and A. Polman, "Design principles for particle plasmon enhanced solar cells," *Appl. Phys. Lett.*, vol. 93, no. 19, pp. 191113, 2008.

[2] F. P. G. de Arquer, and G. Konstantatos, "Metal-insulator-semiconductor heterostructures for plasmonic hot-carrier optoelectronics," *Opt. Exp.*, vol. 23, no. 11, pp. 14715–14723, 2015.

[3] F. Qin *et al.*, "Ultra-broadband and wide-angle perfect solar absorber based on TiN nanodisk and ti thin film structure," *Sol. Energy Mater. Sol. Cells*, vol. 211, pp. 110535, 2020.

[4] T. Guo, "Fiber grating-assisted surface plasmon resonance for biochemical and electrochemical sensing," *J. Lightw. Technol.*, vol. 35, no. 16, pp. 3323–3333, 2017.

[5] X. Wu, J. Zhang, J. Chen, C. Zhao, and Q. Gong, "Refractive index sensor based on surface-plasmon interference," *Opt. Lett.*, vol. 34, no. 3, pp. 392–394, 2009.
[6] Y. M. Qing, H. F. Ma, S. Yu, and T. J. Cui, "Angle-insensitive dual-functional resonators combining cavity mode resonance and magnetic resonance," *Opt. Lett.*, vol. 44, no. 12, pp. 3118–3121, 2019.
[7] F. Sterl, N. Strohfeldt, S. Both, E. Herkert, T. Weiss, and H. Giessen, "Design principles for sensitivity optimization in plasmonic hydrogen sensors," *ACS Sensors*, vol. 5, no. 4, pp. 917–927, 2020.
[8] X. Luo, D. Tsai, M. Gu, and M. Hong, "Subwavelength interference of light on structured surfaces," *Adv. Opt. Photon.,* vol. 10, no. 4, pp. 757–842, 2018.
[9] N. Lawrence, and L. D. Negro, "Radiation rate enhancement in subwavelength plasmonic ring nanocavities," *Nano Lett.,* vol. 13, no. 8, pp. 3709–3715, 2013.
[10] D. Liu *et al.*, "Probing the in-plane near-field enhancement limit in a plasmonic particle-on-film nanocavity with surface-enhanced raman spectroscopy of graphene," *ACS Nano*, vol. 13, no. 7, pp. 7644–7654, 2019.
[11] M. S. Nezami, D. Yoo, G. Hajisalem, S.-H. Oh, and R. Gordon, "Gap plasmon enhanced metasurface third-harmonic generation in transmission geometry," *ACS Photon.,* vol. 3, no. 8, pp. 1461–1467, 2016.
[12] N. Chauvet *et al.*, "Hybrid KTP–plasmonic nanostructures for enhanced nonlinear optics at the nanoscale," *ACS Photon.,* vol. 7, no. 3, pp. 665–672, 2020.
[13] V. J. Sorger, R. F. Oulton, J. Yao, G. Bartal, and X. Zhang, "Plasmonic fabry-pérot nanocavity," *Nano Lett.*, vol. 9, no. 10, pp. 3489–3493, 2019.
[14] N. I. Landy, S. Sajuyigbe, J. J. Mock, D. R. Smith, and W. J. Padilla, "Perfect metamaterial absorber," *Phys. Rev. Lett.*, vol. 100, no. 20, pp. 207402, 2008.
[15] H. Wang, and L. Wang, "Perfect selective metamaterial solar absorbers," *Opt. Exp.*, vol. 21, no. S6, pp. A1078–A1093, 2013.
[16] N. Muhammad, Z. Ouyang, X. Tang, and Q. Liu, "Broadband wide-angle incident light absorption by metallic loop metasurfaces based on electro-optic substrate," *IEEE Photon. Technol. Lett.*, vol. 31, no. 13, pp. 1068–1071, 2019.
[17] K. Aydin, V. E. Ferry, R. M. Briggs, and H. A. Atwater, "Broadband polarization-independent resonant light absorption using ultrathin plasmonic super absorbers," *Nature Commun.*, vol. 2, no. 1, pp. 517, 2011.
[18] C. Ji, K.-T. Lee, T. Xu, J. Zhou, H. J. Park, and L. J. Guo, "Engineering light at the nanoscale: Structural color filters and broadband perfect absorbers," *Adv. Opt. Mater.*, vol. 5, no. 20, pp. 1700368, 2017.
[19] S. Luo, J. Zhao, D. Zuo, and X. Wang, "Perfect narrow band absorber for sensing applications," *Opt. Exp.*, vol. 24, no. 9, pp. 9288–9294, 2016.
[20] X. Wang *et al.*, "A novel plasmonic refractive index sensor based on gold/silicon complementary grating structure," *Chin. Phys. B*, vol. 30, no. 2, pp. 024207, 2021.
[21] Z. Vafapour, "Polarization-independent perfect optical metamaterial absorber as a glucose sensor in food industry applications," *IEEE Trans. Nanobiosci.*, vol. 18, no. 4, pp. 622–627, 2019.
[22] C. Chen, G. Wang, Z. Zhang, and K. Zhang, "Dual narrow-band absorber based on metal–insulator–metal configuration for refractive index sensing," *Opt. Lett.*, vol. 43, no. 15, pp. 3630–3633, 2018.
[23] W. Li, and J. Valentine, "Metamaterial perfect absorber based hot electron photodetection," *Nano Lett.*, vol. 14, no. 6, pp. 3510–3514, 2014.
[24] A. Ghobadi, H. Hajian, B. Butun, and E. Ozbay, "Strong light–matter interaction in lithography-free planar metamaterial perfect absorbers," *ACS Photon.,* vol. 5, no. 11, pp. 4203–4221, 2018.
[25] J. Zhou *et al.*, "Metamaterial and nanomaterial electromagnetic wave absorbers: Structures, properties and applications," *J. Mater. Chem. C*, vol. 8, no. 37, pp. 12768–12794, 2020.
[26] L. Zhou *et al.*, "3D self-assembly of aluminium nanoparticles for plasmon-enhanced solar desalination," *Nature Photon.*, vol. 10, no. 6, pp. 393–398, 2016.
[27] X. Wang, Y. He, X. Liu, G. Cheng, and J. Zhu, "Solar steam generation through bio-inspired interface heating of broadband-absorbing plasmonic membranes," *Appl. Energy*, vol. 195, pp. 414–425, 2017.
[28] P. Tao *et al.*, "Solar-driven interfacial evaporation," *Nature Energy*, vol. 3, no. 12, pp. 1031–1041, 2018.
[29] W. Shang, and T. Deng, "Solar steam generation: Steam by thermal concentration," *Nature Energy*, vol. 1, pp. 16133, 2016.
[30] J. W. Park *et al.*, "Multi-band metamaterial absorber based on the arrangement of donut-type resonators," *Opt. Exp.*, vol. 21, no. 8, pp. 9691–9702, 2013.
[31] L. Zhao, H. Liu, Z. He, and S. Dong, "Theoretical design of twelve-band infrared metamaterial perfect absorber by combining the dipole, quadrupole, and octopole plasmon resonance modes of four different ring-strip resonators," *Opt. Exp.*, vol. 26, no. 10, pp. 12838–12851, 2018.
[32] B. X. Wang, X. Zhai, G. Z. Wang, W. Q. Huang, and L. L. Wang, "Design of a four-band and polarization-insensitive terahertz metamaterial absorber," *IEEE Photon. J.,* vol. 7, no. 1, 2015, Art. no. 4600108.
[33] D. Hu, H. Wang, and Q. Zhu, "Design of six-band terahertz perfect absorber using a simple U-shaped closed-ring resonator," *IEEE Photon. J,* vol. 8, no. 2, 2016, Art. no. 5500608.
[34] Z. Li, S. Butun, and K. Aydin, "Ultranarrow band absorbers based on surface lattice resonances in nanostructured metal surfaces," *ACS Nano*, vol. 8, no. 8, pp. 8242–8248, 2014.
[35] Z. Li, S. Butun, and K. Aydin, "Large-area, lithography-free super absorbers and color filters at visible frequencies using ultrathin metallic films," *ACS Photon.,* vol. 2, no. 2, pp. 183–188, 2015.
[36] D. Zhao *et al.*, "Ultra-narrow-band light dissipation by a stack of lamellar silver and alumina," *Appl. Phys. Lett.*, vol. 104, no. 22, pp. 221107, 2014.
[37] B. Liu *et al.*, "A plasmonic sensor array with ultrahigh figures of merit and resonance linewidths down to 3 nm," *Adv. Mater.*, vol. 30, no. 12, pp. 1706031, 2018.
[38] Z. Liu, G. Liu, G. Fu, X. Liu, Z. Huang, and G. Gu, "All-metal meta-surfaces for narrowband light absorption and high performance sensing," *J. Phys. D: Appl. Phys.*, vol. 49, no. 44, pp. 445104, 2016.
[39] J. Gao *et al.*, "Cavity-driven hybrid plasmonic ultra-narrow bandpass filter," *Opt. Exp.*, vol. 27, no. 15, pp. 20397–20411, 2019.

[40] X. Xiong *et al.*, "Polarization-dependent perfect absorbers/reflectors based on a three-dimensional metamaterial," *Phys. Rev. B*, vol. 88, no. 11, pp. 115105, 2013.

[41] Q. Shen, A. M. Boyce, G. Yang, and M. H. Mikkelsen, "Polarization-controlled nanogap cavity with dual-band and spatially overlapped resonances," *ACS Photon.,* vol. 6, no. 8, pp. 1916–1921, 2019.

[42] W. Liu, and Z. Y. Song, "Terahertz absorption modulator with largely tunable bandwidth and intensity," *Carbon*, vol. 174, pp. 617–624, 2021.

[43] Z. Song, A. Chen, and J. Zhang, "Terahertz switching between broadband absorption and narrowband absorption," *Opt. Exp.*, vol. 28, no. 2, pp. 2037–2044, 2020.

[44] X. Lu, L. Zhang, and T. Zhang, "Nanoslit-microcavity-based narrow band absorber for sensing applications," *Opt. Exp.*, vol. 23, no. 16, pp. 20715–20720, 2015.

[45] L. Bibbò, K. Khan, Q. Liu, M. Lin, Q. Wang, and Z. Ouyang, "Tunable narrowband antireflection optical filter with a metasurface," *Photon. Res.*, vol. 5, no. 5, pp. 500–506, 2017.

[46] N. Muhammad, Z. Ouyang, X. Tang, and Q. Liu, "Broadband wide-angle incident light absorption by metallic loop metasurfaces based on electro-optic substrate," *IEEE Photon. Technol. Lett.*, vol. 31, no. 13, pp. 1068–1071, 2019.

[47] C. J. Tang, Z. L. Wang, W. Y. Zhang, N. B. Ming, G. Sun, and P. Sheng, "Localized and delocalized surface-plasmon-mediated light tunneling through monolayer hexagonal-close-packed metallic nanoshells," *Phys. Rev. B*, vol. 80, no. 16, 165401, 2009, Art. no. 165401.

[48] X. Chen, N. C. Lindquist, D. J. Klemme, P. Nagpal, D. J. Norris, and S.-H. Oh, "Split-wedge antennas with sub-5 nm gaps for plasmonic nanofocusing," *Nano Lett.*, vol. 16, no. 12, pp. 7849–7856, 2016.

[49] L. Qin *et al.*, "5 nm Nanogap electrodes and arrays by Super-resolution laser lithography," *Nano Lett.*, vol. 20, no. 7, pp. 4916–4923, 2020.

[50] A. Kim *et al.*, "Cascade domino lithography for extreme photon squeezing," *Mater. Today*, vol. 39, pp. 89–97, 2020.

[51] D. Ji *et al.*, "Efficient mid-infrared light confinement within sub-5-nm gaps for extreme field enhancement," *Adv. Opt. Mater.*, vol. 5, no. 17, 2017, Art. no. 1700223..

[52] A. Roszkiewicz, and W. Nasalski, "Reflection suppression and absorption enhancement of optical field at thin metal gratings with narrow slits," *Opt. Lett.*, vol. 37, no. 18, pp. 3759–3761, 2012.

[53] R. Walther *et al.*, "Coupling of surface-plasmon-polariton-hybridized cavity modes between submicron slits in a thin gold film," *ACS Photon.*, vol. 3, no. 5, pp. 836–843, 2016.

[54] Q. Min, and R. Gordon, "Surface plasmon microcavity for resonant transmission through a slit in a gold film," *Opt. Exp.*, vol. 16, no. 13, pp. 9708–9713, 2008.

[55] Z. Liu, E. Gao, and F. Zhou, "Sharp multiple-phase resonances in a plasmonic compound grating with multislits," *IEEE Photon. J*, vol. 10, no. 4, 2018, Art. no. 5700508.

[56] A. P. Hibbins, M. J. Lockyear, and J. R. Sambles, "The resonant electromagnetic fields of an array of metallic slits acting as fabry–perot cavities," *J. Appl. Phys.*, vol. 99, no. 12, 2006, Art. no. 124903.